Intelligent Transportation and Smart Cities
V. Mezhuyev et al. (Eds.)

doi:10.3233/ATDE240392

Exploring the Structural Optimization of T-Steel Structure Nodes and the Application of Smart Sensors in Smart Cities

Yuhuai PENG[1] and Jinsong LEI
School of Civil Engineering and Architecture, Southwest University of Science and Technology, Mianyang, Sichuan, China

Abstract. The utilization of semi-rigidly connected T-nodes in architectural engineering projects within smart cities presents advantages such as improved fatigue life of the structure, enhanced adaptability to the long-term development needs of the urban environment, and increased flexibility and construction convenience for smart city development. Additionally, this discussion delves into the application and arrangement of smart sensors on T-nodes, along with the implementation of a stress-strain cloud monitoring system for T-nodes. To comprehensively understand the impact of T-node flange plate thickness and bolt preload on the internal force of T-node bolts, a series of tensile tests and finite element simulation analyses are conducted on the T-node. These analyses aim to derive the load-strain curve of the T-node, providing valuable insights into the influence laws associated with these design parameters.

Keywords. Smart city, smart sensor, steel structure, bolt preload, t-node

1. Introduction

In the construction of smart cities, the design of the beam-column node's connection form plays a pivotal role. Its application not only impacts the safety and stability of the building but is also intricately linked to the sustainable development of the city and the quality of the living environment. The connection methods for beam-column nodes primarily encompass completely rigid, semi-rigid, and articulated connections. Semi-rigid connections, positioned between fully rigid and fully articulated connections, bear significant positive implications in the realm of architectural engineering within smart cities [1-8]. A defining characteristic of smart city is the efficiency and flexibility of building structures, precisely met by semi-rigid connections. In contrast to fully rigid and fully articulated connections, semi-rigid connections exhibit limited elastic deformation in the degrees of freedom of connected members while maintaining certain bending and torsional stiffness. This trait allows the structure to dissipate energy during deformation, effectively mitigating the issue of node stress concentration, thereby reducing stress levels and strain energy within the structure. The use of semi-rigid connections in construction projects in smart cities is observed to enhance the fatigue life of structures, better adapting to the long-term development needs of the urban environment. Moreover, semi-rigid connections offer numerous advantages in

[1] Corresponding Author: Yuhuai PENG, pengyh1089@163.com.

construction. Their deformation capacity facilitates easier adjustment and adaptation to various complex conditions during the building construction process, providing flexibility and construction convenience for the construction of smart cities. Therefore, semi-rigid connections hold considerable application significance in the field of construction engineering in smart cities, injecting new vitality into the sustainable development of the city and the safety of building structures [9-15].

The initiation of a smart sensor network marks the initial phase towards achieving the health monitoring of urban structures. In this study, we will conduct tensile tests and ABAQUS finite element simulation analyses on multiple T-type members to assess the impact of flange plate thickness and bolt preload on the mechanical properties of T-type nodes. Simultaneously, we will integrate intelligent sensors with T-type node members, incorporating various sensor types such as miniature strain sensors, temperature sensors, and accelerometers. These sensors will be strategically placed in T-type nodes to observe the real-time bending deformation of the T-type member, as well as monitor prying force, temperature, axial stress, and bending strain of bolts. This integration aims to establish a comprehensive real-time monitoring system, facilitating the observation of structure deformation and stress distribution while enabling the timely detection of potential issues.

2. Application of Smart Sensors with T-beam Nodes

Smart sensors capitalize on the unique property of certain substances, where their electrical characteristics undergo changes in response to alterations in the surrounding environment. Exploiting this property, smart sensors can convert the physical or chemical quantity being measured into an electrical signal. This signal is then handed over to a data processing subsystem, which executes a series of operations, including signal conditioning, digitization, processing, and in-depth analysis. The primary objective of this process is to transform environmental information into a digitally processable form, providing precise data support for subsequent applications. Upon data processing, smart sensors transmit the processed data to external systems or devices through a communication interface, facilitating efficient connection and information exchange with external systems. It's noteworthy that smart sensors extend beyond basic data conversion and transmission functions, incorporating advanced features such as automatic zero calibration, diagnostic capabilities, and adaptability. These intelligent attributes empower sensors to automatically adjust their operating parameters and status in response to environmental changes and specific needs. This adaptive capability significantly enhances the reliability and adaptability of the system, thereby providing trustworthy monitoring and control support across various application scenarios. This highly intelligent sensor technology holds crucial application value in the field of civil engineering, offering advanced functionalities that contribute to the efficiency, adaptability, and reliability of monitoring and control systems.

2.1. Applications of Miniature Strain Sensors

The occurrence of plastic hinges, particularly at the flange plates of T-beam nodes, poses a critical risk to the structural safety. To effectively monitor this vulnerable area, we opted to install miniature strain sensors at these locations. The selection of these

sensors is based on their high sensitivity, compact design, and adaptability, enabling accurate detection of small deformations and strains. Employing an Internet strain monitoring system, we achieve real-time monitoring of T-beam node flange plates. This automated system efficiently collects and transmits data acquired by miniature strain sensors in real-time. Through comprehensive data analysis, we deduce the stress values at the most critical cross-section of the T-beam node, specifically at the flange plate position. This real-time monitoring and data analysis approach provides a scientific and efficient means of assessing structural safety. The feedback from the monitoring system allows for a more accurate understanding of the stress distribution in the structure under actual loading conditions. Particularly in areas prone to plastic hinges, the timely acquisition of strain data offers prompt and accurate insights into the structural health. Ultimately, the monitored stress values can be compared and evaluated alongside bolt load capacity design values. If the monitoring system indicates that stress values in a specific area exceed the design limits, it suggests potential structural danger. In such cases, decisions regarding reinforcement and repair can be made based on monitoring results, further enhancing the safety and reliability of the structure.

2.2. Application of Piezoelectric Smart Gasket Sensors

The piezoelectric smart gasket sensor represents a thin film-like sensor leveraging piezoelectric materials to measure the tightening state and load distribution of bolted joints. This capability enables the health monitoring and safety evaluation of bolted structures. The sensor can be strategically mounted on the contact surface of the bolt. By sensing strain and vibration, it can capture subtle bolt deformations and provide instantaneous status feedback by connecting to a real-time monitoring system. The real-time monitoring system is equipped to set alarm thresholds, activating the alarm system when abnormal bolt deformation or vibration is detected to prompt timely corrective action. Harnessing the adaptive nature of the sensor, the system can automatically adjust working parameters based on the monitored bolt status, ensuring prompt and effective anti-loosening measures. In-depth analysis of data acquired by the sensors through data analytics tools facilitates the prediction of bolt life, early identification of potential issues, and the planning of maintenance measures. This integrated approach to smart sensing technology not only effectively prevents bolt loosening problems but also enhances the safety and reliability of the structure.

3. Overview of T-node Tests

3.1. Specimen Design

Three specimens were designed for this test, utilizing high-strength 10.9-grade bolts with a 16 mm diameter [16-18]. The specimen design primarily focused on the flange plate thickness parameter. Detailed dimensions of the specimens are presented in Table 1 and Figure 1 below.

Table 1. T-node dimension table

Specimen No.	Geometric Dimensions					Bolt preload/kN
	t_f/mm	t_w/mm	e_n/mm	e_w/mm	b/mm	
P0	16	16	75	75	100	0
P1	16	16	75	75	100	100
P2	16	16	75	75	100	150

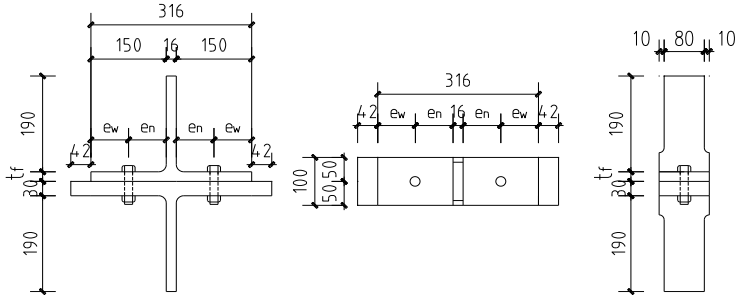

Figure 1. Diagrammatic representation of the specimen, including the main view, top view, and left view.

3.2. Calculation Method of Bolt Internal Force

Bolt strain measurement points are illustrated in Figure 2. Due to the specimen's symmetrical structure, under ideal conditions, the deformation of the two bolts is symmetrical. Consequently, the strain values at symmetrical points on the specimen, such as measurement point 1 and measurement point 4, measurement point 2 and measurement point 3, are equal after force application. Therefore, in this study, the average strain value of measuring point 1 and measuring point 4 is defined as ε_1, and the average strain value of measuring point 2 and measuring point 3 is defined as ε_2. The fundamental relationship between stress and strain is then expressed as:

$$\sigma = f(\varepsilon) = \begin{cases} \varepsilon E & \varepsilon \le \varepsilon_0 \\ \varepsilon_0 E + E_t(\varepsilon - \varepsilon_0) & \varepsilon > \varepsilon_0 \end{cases} \tag{1}$$

In Equation 1, ε represents the surface strain measured by the strain gauge, while ε0 denotes the yield strain of the bolt. σ1=f (ε1) represent the outer stress of the bolt, and σ2=f(ε2) represent the inner stress of the bolt. Within the elastic range, can be calculated using Equation 2. This equation facilitates the conversion of unevenly distributed stress into the sum of axial stress and bending stress.

$$\begin{cases} \sigma_{\text{Axial stress}} = \dfrac{\sigma_1 + \sigma_2}{2} \\ \sigma_{\text{Bending stress}} = \dfrac{\sigma_2 - \sigma_1}{2} \end{cases} \tag{2}$$

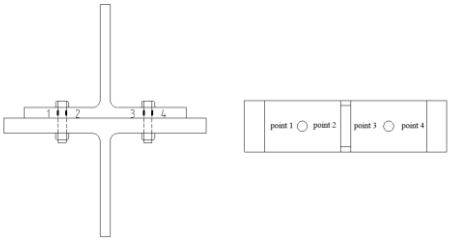

Figure 2. Schematic diagram of strain gage adhesion on specimen.

4. T-node Tensile Test

4.1. Material Properties Test

To gain a comprehensive understanding of the mechanical properties of the materials, we conducted material properties tests on steels with varying thicknesses and strengths. These tests provided detailed performance indicators, including the modulus of elasticity (E), yield strength (f_y), ultimate strength (f_u), and elongation of the steel. It is noteworthy that the material used for the T-beam is Q345, and the high-strength bolts are of grade 10.9. Furthermore, standardized specimens of the section steel were processed. The material property parameters obtained following the tensile testing of standard specimens for steel sections are presented in Table 2 below:

Table 2. Results of material performance testing

Specimen No.	Yield load F_y(kN)	Limit load F_u(kN)	Yield strength f_y(MPa)	Limit strength f_u(MPa)	Modulus of elasticity E(MPa)
Q345	112.23	170.66	351.36	536.25	203633.2

The material parameters for 10.9-grade high-strength bolts, obtained from the product quality assurance certificate, are reflected in the values presented in Table 3 below:

Table 3. Mechanical properties of 10.9 grade high-strength bolt materials

Yield strength f_y(MPa)	Limit strength f_u(MPa)	Modulus of elasticity E(MPa)	Elongation (%)
950	1080	2.06 × 105	12

4.2. Experimental Phenomena

Before loading, specimen P0 experienced rapid detachment of the T-node flange plate from the base steel plate due to the absence of bolt preload. Midway through the loading process, a slight tensile phenomenon became visible. As the load increased gradually, the T-node flange plate exhibited bending deformation. Eventually, the left side of the specimen suddenly buckled, and the threads were damaged, leading to the halt of the test equipment loading. Refer to Figure 3 for detailed observations.

Specimen P1 was subjected to a preload force of 100 kN. Initially, during the loading commencement, the T-node flange plate was in close contact with the base steel plate. As the loading force increased, the T-node flange plate exhibited a slight expansion. Ultimately, most of the strain gauges failed, leading to the conclusion of the test. Refer to Figure 4 for detailed illustrations.

Specimen P2 was subjected to a preload force of 150 kN. Prior to the application of the load, the flange plate and the base plate were maintained in close contact. With the gradual increase of the load, towards the end of the loading period, the flange plate of the T-node exhibited a subtle tensioning phenomenon that was challenging to detect visually. Ultimately, the strain gauges failed, leading to the cessation of the loading on the test equipment. Refer to Figure 5 for detailed visual representation.

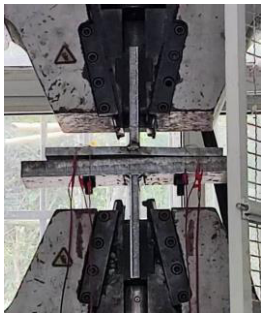

Figure 3. Phenomena observed in the P0 specimen test

Figure 4. Phenomena observed in the P1 specimen test

Figure 5. Phenomena observed in the P2 specimen test

4.3. Results and Analysis

4.3.1. The influence of bolt preload

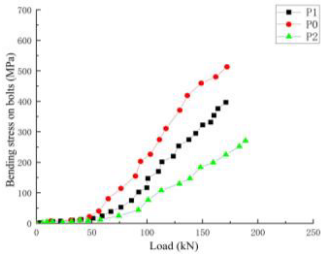

(a) Load-bending stress on bolts curves P0, P1, P2

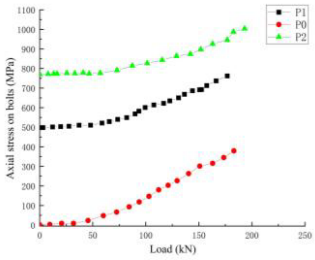

(b) Load-axial stress on bolts curves P0, P1, P2

Figure 6. Test results for specimens P0, P1, P2.

In Figure 6 (a) (b), it is evident that the bolt bending stress of specimen P0 not only exhibits the fastest growth but also attains the highest magnitude. This can be attributed to the absence of preload in specimen P0, resulting in a weakened connection between the bolt and the T-beam node. Consequently, the T-beam node is more susceptible to bending. Conversely, specimens with higher preload showcased higher initial axial stresses before loading, a result of the mutual extrusion between bolts and T-beam nodes. The axial stress of specimen P0 also experiences the most rapid increase as the load escalates but consistently remains lower than that of specimens P1 and P2. This observation indicates that smaller bolt preloads correlate with higher bolt bending stress in the T-steel node, leading to more pronounced bending deformation of the T-steel node.

5. Finite Element Simulation of T-nodes

5.1. Introduction

Finite element software plays a crucial role in various aspects of smart city construction engineering, utilizing its robust analysis capabilities. T-node forces are intricate, requiring a detailed study of their mechanical properties. This chapter employs ABAQUS finite element software for simulation and analysis, allowing for a comprehensive understanding of T-node behavior. Modeling with ABAQUS enables not only the simulation of the entire test process but also provides a clearer view of intricate details that may be challenging to capture in physical tests [19-21]. This approach aims to achieve sustainable development in the realm of smart city construction engineering.

5.2. Test Piece Design

To ensure the accuracy of the finite element model, a comparison between Base simulation results and test outcomes was conducted. Additionally, to explore the impact of and bolt preload on ultimate load capacity, yield load, initial stiffness, and bolt internal force, three specimens were designed for finite element simulation. The detailed dimensions of these specimens are outlined in Table 4 below:

Table 4. T-node dimension table

Specimen No.	Flange Plate Thickness (t_f/mm)	Web Plate Thickness (t_w/mm)	Bolt Diameter (d/mm)	Width of Plate (b/mm)
P1	16	16	16	100
T1	12	16	16	100
T2	20	16	16	100

5.3. Modeling

The selected finite element modeling unit for this study is C3D8R, an eight-node linear reduced-integral hexahedral unit known for its efficiency and accuracy in managing nonlinear geometric problems. In the model, the bolt rods are represented as equal-diameter cylinders, while the nuts take the form of positive hexagonal cylinders. The mesh model for T-nodes is detailed in Figures 7 and 8.

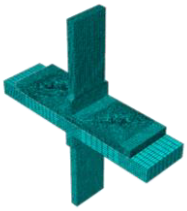

Figure 7. Mesh division of t-node

Figure 8. Mesh delineation of high-strength bolts

5.4. Parameter Analysis

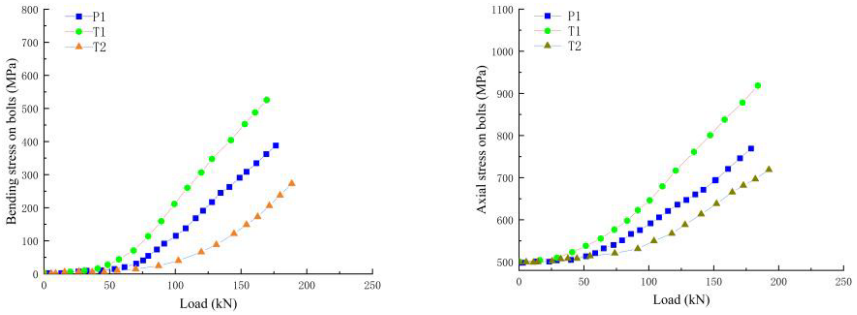

(a) Load-bending stress on bolts curves P1, T1, T2 (b) Load-axial stress on bolts curves P1, T1, T2

Figure 9. Load stress curves for specimen P1, T1, T2.

As depicted in Figure 9, this set of ABAQUS simulations primarily focuses on the variation of the airfoil thickness. Specimens P1 and T2 exhibit higher flexural stiffness attributed to their larger flange thickness, resulting in a reduction of the bending moment on the bolts. In contrast, specimen T1 is more susceptible to bending under load due to its thin flange plate. Therefore, under equivalent loads, a thinner flange plate in the T-node increases the likelihood of flange plate bending deformation, consequently leading to an elevation in the bending moment of the bolt.

6. Conclusions

In this study, tensile tests and ABAQUS finite element simulation analyses were conducted primarily on three T-nodes to explore the impact of flange plate thickness on the ultimate load-carrying capacity and bolt internal force of T-nodes. The following conclusions have been drawn:

- The presence of bolt preload serves as effective anchoring for the T-node, simultaneously reducing the growth rate of bending stress and axial stress. However, it's crucial to note that a larger preload doesn't necessarily equate to better performance for the T-node. Excessive preload can lead to a higher axial pressure on the bolts, increasing the risk of bolt failure.
- The thickness of the flange plate in the T-node directly influences its bearing capacity. A greater thickness enhances the overall bearing capacity, providing better protection for the bolts and extending their service life.
- In areas prone to plastic hinges in the T-node, the addition of miniature strain sensors allows for real-time monitoring. The timely acquisition of strain data provides accurate feedback on the structural health. The monitored stress values can then be compared and evaluated in conjunction with the design value of the bolt load capacity.
- The judicious use of piezoelectric smart shim sensors to monitor bolt preload values prevents bolt loosening and detachment, enhancing the safety and reliability of the steel nodes and, consequently, the entire structure.

The construction of smart cities is intricately linked to T-nodes, acting as key components that support city infrastructure and enable real-time monitoring, early warning, and maintenance through IoT and big data technologies. Thoughtful T-node design, considering their synergy with other city systems, is crucial for effective smart city construction. This holistic design approach optimizes urban structures, enhancing adaptability to future technological developments and urban sustainability requirements.

References

[1] AlAwadhi S, Scholl HJ. Aspirations and Realizations: The Smart City of Seattle. 46th Annual Hawaii International Conference on System Sciences (HICSS), 2013: 1695-1703.
[2] Angelidou M. Smart city planning and development shortcomings. TeMA-Journal of Land Use, Mobility and Environment, 2017, 10(1): 77-94.
[3] Bălăşescu S, Neacşu NA, Madar A, Zamfirache A, Bălăşescu M. Research of the Smart City Concept in Romanian Cities. Sustainability, 2022, 14(16): 10004.
[4] Dai Y, Hasanefendic S, Bossink B. A Systematic Literature Review of the Smart City Transformation Process: The Role and Interaction of Stakeholders and Technology. Sustainable Cities and Society, 2024, 101: 105112.
[5] Gupta N. Editorial: Smart Cities Challenges, Technologies and Trends. Frontiers in Big Data, 2023, 6: 1258051-1258051.
[6] Hoffman MC. Smart Cities: A Review of the Most Recent Literature. Informatization Policy, 2020, 27(1): 003-035.
[7] Kirimtat A, Krejcar O, Kertesz A, Tasgetiren MF. Future Trends and Current State of Smart City Concepts: A Survey. Ieee Access, 2020, 8: 86448-86467.
[8] Lin X, Quan H, Zhang H, Huang Y. The 5I model of smart city: A case of Shanghai, china. 2015 IEEE first international conference on big data computing service and applications. IEEE, 2015: 329-332.
[9] Komninos N, Kakderi C, Panori A, Tsarchopoulos P. Smart city planning from an evolutionary perspective. Journal of Urban Technology, 2019, 26(2): 3-20.
[10] Liu Y, Ye M. Analysis on the Development of Smart City of Big Cities in China and Its Effect to Economic Structure Based on Entropy Method. Security and Communication Networks, 2022, 2022.
[11] Mohanty SP. Low-Cost Consumer Technology Can Help to Build Sustainable Smart Villages. IEEE Consumer Electronics Magazine, 2021, 10(3): 4-5.
[12] Noori N, Hoppe T, De Jong M. Classifying Pathways for Smart City Development: Comparing Design, Governance and Implementation in Amsterdam, Barcelona, Dubai, and Abu Dhabi. Sustainability, 2020, 12(10): 4030.
[13] Orlowski A. Smart Cities Concept-Readiness of City Halls as a Measure of Reaching a Smart City Perception. Cybernetics and Systems, 2021, 52(5): 313-327.
[14] Prabowo OM, Mulyana E, Nugraha IG, Supangkat SH. Cognitive City Platform as Digital Public Infrastructure for Developing a Smart, Sustainable and Resilient City in Indonesia. IEEE Access, 2023, 11: 120157-120178.
[15] Samarakkody A, Amaratunga D, Haigh R. Characterising Smartness to Make Smart Cities Resilient. Sustainability, 2022, 14(19): 12716.
[16] Khani R, Hosseinzadeh Y, Asl MH. Investigating the prying force magnitude and location in the T-stub connection based on the energy method. Engineering Structures, 2023, 280: 115655.
[17] Nair RS, Birkemoe PC, Munse WH. High strength bolts subject to tension and prying. Journal of the Structural Division, 1974, 100(2): 351-372.
[18] El Kalash SN, Hantouche EG. Prying effect in unstiffened extended endplate connection with circular bolts configuration. Journal of Constructional Steel Research, 2019, 160: 402-410.
[19] Francavilla AB, Latour M, Piluso V, et al. Simplified finite element analysis of bolted T-stub connection components. Engineering Structures, 2015, 100: 656-664.
[20] Bezerra LM, Bonilla J, Silva WA, et al. Experimental and numerical studies of bolted T-stub steel connection with different flange thicknesses connected to a rigid base. Engineering structures, 2020, 218: 110770.
[21] Liang G, Guo H, Liu Y, et al. Q690 high strength steel T-stub tensile behavior: Experimental and numerical analysis. Thin-Walled Structures, 2018, 122: 554-571.